Derivation of inelastic-electron-scattering cross sections from quantitative analysis of reflection-electron-energy-loss spectra

Y. F. Chen*
Precision Instrument Development Center, National Science Council, Hsinchu, Taiwan, Republic of China
(Received 19 March 1998)

The inelastic interaction of electrons with solid surfaces is studied within the framework of dielectric response theory. It is shown that the inelastic interaction can be characterized by the differential inverse inelastic mean free path (DIIMFP) for bulk excitations and the differential surface excitation parameter (DSEP) for surface effects. Based on transport theory, the inelastic scattering cross section $K(E_0 \rightarrow E_0-\omega)$ experimentally determined from reflection-electron-energy-loss spectroscopy (REELS) can be related to the bulk DIIMFP and DSEP. From this relation, a method to derive the bulk DIIMFP and DSEP from experimental $K(E_0 \rightarrow E_0-\omega)$ is proposed. With this method, the bulk DIIMFP and DSEP derived from REELS data for Au and Cu are in good agreement with the theoretical results calculated with the model dielectric function.
[S0163-1829(98)07136-7]

I. INTRODUCTION

The information about the inelastic scattering properties of medium energy electrons (200–2000 eV) near solid surfaces is both of fundamental and practical importance due to the fact that surface electron spectroscopies such as Auger-electron spectroscopy (AES) and x-ray photoelectron spectroscopy (XPS) are greatly affected by inelastic-scattering events experienced by electrons. An important quantity in connection with quantitative analysis of surface electron spectroscopies is the differential inverse inelastic mean free path (DIIMFP). Dielectric response theory[1–6] is often used to perform theoretical calculations in which the complex dielectric-response function of the particular solid must be known in detail with respect to energy and momentum transfers. Methods based on model dielectric functions and experimental optical constants have been developed and applied to various solids.[4–10] Nevertheless, a method to assess experimentally the DIIMFP is of great importance for surface analysis and also for fundamental studies of electron-solid interaction.

Previously, transmission electron energy-loss spectroscopy (TEELS) was developed for determining the DIIMFP and optical constants.[11–14] However, a major drawback associated with TEELS is that a transmission electron spectrometer is necessary to provide an incident electron beam greater than 10 keV energy for transmitting the primary electrons through the sample. Besides, the sample must be prepared in the form of a thin, free-standing film (less than 2000 Å) that limits the types of materials that can be studied using TEELS.

Reflection electron energy-loss spectroscopy[15–20] (REELS) was used to solve experimental limitations associated with TEELS. In general, primary electron energies used in REELS is less than 2 keV; thus, standard electron spectrometers equipped with Auger-electron sources can be used. Tougaard and co-workers[21–23] have pioneered the application of REELS experiments to gain knowledge about inelastic scattering cross sections, $K(E_0 \rightarrow E_0-\omega)$. Here E_0 is the incident electron energy and ω is the electron-energy loss. The experimentally determined $K(E_0 \rightarrow E_0-\omega)$ are significantly different from the conventional DIIMFP for bulk excitations due to the effect of surface excitations.[4–6,23–25] The method of Tougaard and Chorkendorff becomes especially attractive because the determined DIIMFP may be applied to remove the inelastic background signal from AES or XPS spectra.[21,22,26,27] However, an inherent problem is that $K(E_0 \rightarrow E_0-\omega)$ determined from REELS data contain information associated with electrons traversing the solid-vacuum surface twice while, in the AES or XPS measurement, the signal electrons traverse this surface only once. As a result, the intensities associated with surface excitations in REELS spectra are enhanced with respect to the AES or XPS measurement.[28,29]

Recently, Yubero and co-workers[4,30] proposed a model to reproduce $K(E_0 \rightarrow E_0-\omega)$ with dielectric theory and a weight function. They assumed $K(E_0 \rightarrow E_0-\omega)$ to be a genuine single-inelastic-scattering cross section; thus, the probability function that the electron has undergone a single inelastic scattering event was used to average over all possible paths. However, $K(E_0 \rightarrow E_0-\omega)$ is not a pure single-inelastic-scattering cross section due to the contribution of surface excitations. Besides, the model of Yubero and co-workers cannot be used to separate the surface and bulk components from $K(E_0 \rightarrow E_0-\omega)$ due to their assumption, even though this model presents a good agreement with experimental data. Considering the difference in surface effects between REELS and AES as well as XPS, a method for separation of the contribution of the bulk and surface excitations from experimentally determined $K(E_0 \rightarrow E_0-\omega)$ is essential to obtain quantitative knowledge for surface electron spectroscopies. Moreover, if the DIIMFP for bulk excitations is isolated over a large energy range, one may determine the complex dielectric function through a Kramers-Kroning analysis.[11–14]

In this work, we used dielectric response theory to derive the DIIMFP for electrons obliquely passing through the solid surface. It was found that the derived DIIMFP can be divided

into a bulk and a surface term. The bulk term is the DIIMFP in an infinite medium, while the surface term is spatially varying on both sides of the vacuum-solid surface. Since surface effects are restricted to a surface layer on the order of several angstroms, these effects can be described by the differential surface excitation parameter (DSEP) which is the integration of the surface term in the DIIMFP. Including surface effects into the quantitative analysis, experimental $K(E_0 \rightarrow E_0-\omega)$ can be related to the bulk DIIMFP and DSEP. With this derived relation, the bulk DIIMFP and DSEP can be directly determined using the experimental $K(E_0 \rightarrow E_0-\omega)$ at two different primary electron energies without any other input parameter. The bulk DIIMFP and DSEP determined from REELS data for Au and Cu are presented and compared to the theoretical results calculated with the model dielectric function.[5,10,25]

II. INELASTIC ELECTRON INTERACTIONS IN SOLID SURFACES

The specular-reflection model (SRM) of Ritchie and Marusak[31] is known to reproduce very well many properties of real surfaces by expressing the surface response in terms of the bulk dielectric function.[32–35] In this model, the medium is described by a ''jellium'' in which the surface is assumed to be abruptly terminated and the constitute electrons of the medium incident on the surface rebound in a specular fashion.[36,37] Although quantum-mechanical analyses can result in a more rational condition of the behavior of constituent electrons at surfaces,[3] the resulting expressions are much less transparent than the semiclassical dielectric theory and probably too cumbersome for use in surface electron spectroscopies. Previously, the SRM has been used to analyze the configuration of the specular reflecting trajectory of an external incident electron.[32–35] In this work, we shall restrict ourselves to the penetrating trajectory of the external incident electron that is a typical spectroscopic experiment involving fast electrons.

We have recently derived the spatially varying DIIMFP of an electron penetrating into vacuum from a solid for quantitative analysis of XPS.[5,10] Since the electron trajectories in a REELS experiment include incoming (IN) and outgoing (OUT) trajectories, it is convenient to consider the general case of two adjacent materials separated by a planar interface and characterized by the dielectric response function $\varepsilon_a(\mathbf{q},\omega)$ and $\varepsilon_b(\mathbf{q},\omega)$. The interface will be chosen at the plane $z=0$ with the z axis in the perpendicular direction from medium $\varepsilon_a(\mathbf{q},\omega)$ to medium $\varepsilon_b(\mathbf{q},\omega)$. The notation $\nu=|\boldsymbol{\nu}|$, $\mathbf{q}=(\mathbf{Q},q_z)$, $\boldsymbol{\nu}=(\boldsymbol{\nu}_\parallel,\nu_z)$, and $\mathbf{r}=(\mathbf{R},z)$, where $\mathbf{Q}$, $\boldsymbol{\nu}_\parallel$, and $\mathbf{R}$ represent components parallel to the interface, will be adopted hereafter. Note that atomic units are used through this work, unless otherwise specified.

In the fast-charge approximation, a fast electron which interacts with matter can be considered as a point charge with moving charge density given by $\rho(\mathbf{r},t)=-\delta(\mathbf{r}-\boldsymbol{\nu}t)$.[2,3] For an fast electron passing through the interface at $t=0$ from medium $\varepsilon_a(\mathbf{q},\omega)$ to medium $\varepsilon_b(\mathbf{q},\omega)$, the Fourier components of the scalar electric potential can be expressed by

$$\phi^{(a)}(\mathbf{q},\omega)=\frac{-8\pi^2}{q^2\varepsilon_a(\mathbf{q},\omega)}\,[\,\delta(\omega-\mathbf{q}\cdot\boldsymbol{\nu})+\rho_s(\mathbf{Q},\omega)], \quad (1)$$

$$\phi^{(b)}(\mathbf{q},\omega)=\frac{-8\pi^2}{q^2\varepsilon_b(\mathbf{q},\omega)}\,[\,\delta(\omega-\mathbf{q}\cdot\boldsymbol{\nu})-\rho_s(\mathbf{Q},\omega)]. \quad (2)$$

The first terms in Eqs. (1) and (2) represent the charge density of the moving electron and $\rho_s(\mathbf{Q},\omega)$ is the amplitude of the fictitious surface charge that is required to satisfy the requisite boundary conditions, respectively. The opposite sign of the second term between Eq. (1) and Eq. (2) originates from the requirement of continuity of the electric displacement. Matching $\phi^{(a)}(z=+0)$ and $\phi^{(b)}(z=-0)$ yields the required $\rho_s(\mathbf{Q},\omega)$ as

$$\rho_s(\mathbf{Q},\omega)=\frac{Q}{\pi}\,\frac{|\nu_z|}{\tilde{\omega}^2+(\nu_z Q)^2} \times\frac{\tilde{\varepsilon}_a(\mathbf{Q},\omega)\tilde{\varepsilon}_b(\mathbf{Q},\omega)}{\varepsilon_a(\tilde{\mathbf{q}},\omega)\varepsilon_b(\mathbf{q},\omega)}\,\frac{\varepsilon_a(\tilde{\mathbf{q}},\omega)-\varepsilon_b(\tilde{\mathbf{q}},\omega)}{\tilde{\varepsilon}_a(\mathbf{Q},\omega)+\tilde{\varepsilon}_b(\mathbf{Q},\omega)}, \quad (3)$$

where

$$\frac{1}{\tilde{\varepsilon}_{a,b}(\mathbf{Q},\omega)}=\frac{Q}{\pi}\int_{-\infty}^{\infty}\frac{dq_z}{q^2\varepsilon_{a,b}(\mathbf{q},\omega)}, \quad (4)$$

$\tilde{\omega}=\omega-\boldsymbol{\nu}_\parallel\cdot\mathbf{Q}$ and $\tilde{q}^2=Q^2+\tilde{\omega}^2/\nu_z^2$. In terms of $\rho_s(\mathbf{Q},\omega)$ the induced scalar potential is obtained form Eqs. (1) and (2) as

$$\phi_{\rm ind}(\mathbf{r},t)=\frac{-1}{2\pi^2}\int d\omega\int d^3\mathbf{q}\,\frac{e^{i(q\cdot r-\omega t)}}{q^2} \times\left\{\rho_s(\mathbf{Q},\omega)\left[\frac{\Theta(-z)}{\varepsilon_a(\mathbf{q},\omega)}-\frac{\Theta(z)}{\varepsilon_b(\mathbf{q},\omega)}\right]+\delta(\omega-\mathbf{q}\cdot\boldsymbol{\nu}) \times\left[\left(\frac{\Theta(-z)}{\varepsilon_a(\mathbf{q},\omega)}+\frac{\Theta(z)}{\varepsilon_b(\mathbf{q},\omega)}-1\right)\right]\right\}, \quad (5)$$

where $\Theta(z)$ is the Heaviside step function.

The stopping power is given by[3]

$$-\frac{dW}{ds}=\frac{1}{\nu}\left[\frac{\partial\phi_{\rm ind}(\mathbf{r},t)}{\partial t}\right]_{\mathbf{r}=\boldsymbol{\nu}t}, \quad (6)$$

where the derivative of $\phi_{\rm ind}$ is evaluated at the position of the electron, $\mathbf{r}=\boldsymbol{\nu}t$. From Eqs. (5) and (6) we get the stopping power of the solid for the electron

$$-\frac{dW}{ds}=\frac{i}{2\pi^2 v}\int\omega\,d\omega\int d^2\mathbf{Q}\left\{\frac{\pi}{Q}\,\rho_s(\mathbf{Q},\omega)e^{-i\tilde{\omega}z/v_z} \times\left[\frac{\Theta(-z)}{\tilde{\varepsilon}_a(\mathbf{Q},\omega,z)}-\frac{\Theta(z)}{\tilde{\varepsilon}_b(\mathbf{Q},\omega,z)}\right] +\frac{|\nu_z|}{\tilde{\omega}^2+(\nu_z Q)^2}\left[\frac{\Theta(-z)}{\varepsilon_a(\tilde{\mathbf{q}},\omega)}+\frac{\Theta(z)}{\varepsilon_b(\tilde{\mathbf{q}},\omega)}-1\right]\right\}, \quad (7)$$

where

$$\frac{1}{\overline{\varepsilon}_{a,b}(z,\mathbf{Q},\omega)}=\frac{Q}{\pi}\int_{-\infty}^{\infty}\frac{dq_z e^{iq_z z}}{q^2\varepsilon_{a,b}(q,\omega)}. \tag{8}$$

The evaluation of the first term in the curly bracket of Eq. (7) depends on sgn z, as this determines whether the ω integration must be performed by closing through the upper (U) or lower (L) half-plane (HP). For $z<0$, i.e., the electron inside the medium $\varepsilon_a(\mathbf{q},\omega)$ and approaching the interface, we must close the integration contour through the UHP. On the other hand, for $z>0$, i.e., the electron inside the medium $\varepsilon_b(\mathbf{q},\omega)$ and moving away from the surface, the integration contour must be closed through the LHP. This integration contour involves the poles of $\rho_s(\mathbf{Q},\omega)$ and $1/\overline{\varepsilon}_{a,b}(\mathbf{Q},\omega,z)$, which approach the real axis from below and give the surface and bulk excitation modes of the solid, respectively. For simplicity it is convenient to use the identity[33]

$$e^{-i\tilde{\omega}z/\nu_z}=2\cos(\tilde{\omega}z/\nu_z)-e^{i\tilde{\omega}z/\nu_z}. \tag{9}$$

The integration containing the complex exponential on the right-hand side of Eq. (9) can be then performed again through the UHP. Therefore Eq. (7) can be written as

$$-\frac{dW}{ds}=\frac{1}{\pi^2\nu}\int_0^{\infty}d\omega\int d^2\mathbf{Q}\,\frac{\omega|\nu_z|}{\tilde{\omega}^2+(\nu_z Q)^2}\times\mathrm{Im}\left\{\Pi(\nu,z,\mathbf{Q},\omega)-\left[\frac{\Theta(-z)}{\varepsilon_a(\tilde{\mathbf{q}},\omega)}+\frac{\Theta(z)}{\varepsilon_b(\tilde{\mathbf{q}},\omega)}\right]\right\}, \tag{10}$$

where

$$\Pi(\nu,z,\mathbf{Q},\omega)=\left[\frac{e^{-Q|z|}\Theta(-z)}{\overline{\varepsilon}_a(z,\mathbf{Q},\omega)}-\frac{(2\cos(\tilde{\omega}z/\nu_z)-e^{-Q|z|})\Theta(z)}{\overline{\varepsilon}_b(z,\mathbf{Q},\omega)}\right]\times\left[\frac{\overline{\varepsilon}_a(\mathbf{Q},\omega)\overline{\varepsilon}_b(\mathbf{Q},\omega)}{\varepsilon_a(\tilde{\mathbf{q}},\omega)\varepsilon_b(\tilde{\mathbf{q}},\omega)}\,\frac{\varepsilon_b(\tilde{\mathbf{q}},\omega)-\varepsilon_a(\tilde{\mathbf{q}},\omega)}{\overline{\varepsilon}_a(\mathbf{Q},\omega)+\overline{\varepsilon}_b(\mathbf{Q},\omega)}\right], \tag{11}$$

corresponds to the spatially varying surface energy-loss function. In this derivation we have used the property $\varepsilon_{a,b}(-\mathbf{q},-\omega)=\varepsilon^*_{a,b}(\mathbf{q},\omega)$. The energy and momentum conservation can be included by limiting the range of integration over $\mathbf{Q}$ as follows:

$$q_-^2\leqslant\left(\frac{\tilde{\omega}}{\nu_z}\right)^2+Q^2\leqslant q_+^2, \tag{12}$$

where $q_\pm=\sqrt{2E}\pm\sqrt{2(E-\omega)}$.

For an electron of energy $E=\nu^2/2$ to loss energy ω, the spatially varying DIIMFP, $\mu(E\rightarrow E-\omega,\alpha,z)$, can be related to stopping power as follows:[2]

$$-\frac{dW}{ds}=\int_0^{\infty}\omega\mu(E\rightarrow E-\omega,\alpha,z)d\omega, \tag{13}$$

where α is the angle between the electron velocity and positive z axis. The definition of α will be used hereafter.

The vacuum-solid system is the typical case in REELS experiment. From Eqs. (10)–(13), after some algebra, the DIIMFP for vacuum-solid surface can be split into a bulk and a surface term,

$$\mu(E\rightarrow E-\omega,\alpha,z)=\mu_B(E\rightarrow E-\omega)+\mu_S(E\rightarrow E-\omega,\alpha,z) \tag{14}$$

where

$$\mu_B(E\rightarrow E-\omega)=\frac{1}{\pi^2\nu}\int d^2\mathbf{Q}\,\frac{|\nu_z|}{\tilde{\omega}^2+(\nu_z Q)^2}\,\mathrm{Im}\left[-\frac{\Theta(-z)}{\varepsilon(\tilde{\mathbf{q}},\omega)}\right], \tag{15}$$

and

$$\mu_S(E\rightarrow E-\omega,\alpha,z)=\frac{1}{\pi^2\nu}\int d^2\mathbf{Q}\,\frac{|\nu_z|}{\tilde{\omega}^2+(\nu_z Q)^2}\,\mathrm{Im}[\Pi_s(\boldsymbol{\nu},z,\mathbf{Q},\omega)], \tag{16}$$

where

$$\Pi_s(\boldsymbol{\nu},z,\mathbf{Q},\omega)=e^{-Q|z|}\left\{\Theta(-\boldsymbol{\nu}\cdot\hat{\mathbf{z}})\left[e^{-Q|z|}\Theta(z)-\frac{(2\cos(\tilde{\omega}z/\nu_z)-e^{-Q|z|})\Theta(-z)}{\overline{\varepsilon}(z,\mathbf{Q},\omega)}\right]+\Theta(\boldsymbol{\nu}\cdot\overline{\mathbf{z}})\left[[2\cos(\tilde{\omega}z/\nu_z)-e^{-Q|z|}]\Theta(z)-\frac{e^{-Q|z|}\Theta(-z)}{\overline{\varepsilon}(z,\mathbf{Q},\omega)}\right]\right\}\left[\frac{\overline{\varepsilon}(\mathbf{Q},\omega)}{\varepsilon(\tilde{\mathbf{q}},\omega)}\,\frac{\varepsilon(\tilde{\mathbf{q}},\omega)-1}{\overline{\varepsilon}(\mathbf{Q},\omega)+1}\right]. \tag{17}$$

Here the solid $\varepsilon(\mathbf{q},\omega)$ contained in the region $z<0$ and $\hat{\mathbf{z}}$ is the unit vector of positive z axis. The bulk term which is independent of the position and emission angle gives rise to the well-known expression of the DIIMFP of electrons moving in an infinite medium.[2] The inelastic mean free path (IMFP) for bulk excitations is then given by

$$\lambda_B(E)=\left[\int_0^E d\omega\,\mu_B(E\rightarrow E-\omega)\right]^{-1}. \tag{18}$$

On the other hand, the surface term is not confined to the interior of the solid, but also takes place, while the electron is at some distance outside the surface. Note that the first term inside the curly bracket of Eq. (17) corresponds to the electron moving in the negative z direction, i.e., an IN trajectory ($\pi/2<\alpha<\pi$), whereas the second term corresponds to the electron moving in the positive z direction, i.e., an OUT trajectory ($0<\alpha<\pi/2$).

Since there is the $e^{-Q|z|}$ term in $\Pi_s(\boldsymbol{\nu},z,\mathbf{Q},\omega)$, surface

effects have a rather limited extent about the surface.[5,10] The effective region extends into the solid to a depth about v/ω_p, where ω_p is the plasmon energy.[12] Since ω_p lies in the interval 20–35 eV, the depth is roughly around 3–6 Å for a 1 keV electron. Accordingly, the reflected electrons in REELS experiment nearly penetrate this effective region in both IN and OUT trajectories. Therefore, surface effects can be practically characterized by the DSEP that is calculated via integration of Eq. (16), i.e.,

$$P_S(E\rightarrow E-\omega,\alpha)=\int_{-\infty}^{\infty}\frac{dz}{\cos\alpha}\,\mu_S(E\rightarrow E-\omega,\alpha,z). \tag{19}$$

Even though the interval of the integration in Eq. (19) is infinite, the effective contribution is restricted to a limited region extending on both sides of the vacuum-solid surface. The surface excitation parameter (SEP) for an electron penetrating a vacuum-solid surface is then given by[5,24]

$$P_S(E,\alpha)=\int_0^E P_S(E\rightarrow E-\omega,\alpha)d\omega. \tag{20}$$

The SEP is the probability for a single loss event. The probability of n successive surface plasmons excited by an electron traversing the effective region should obey the Poisson stochastic process:

$$P_n=\frac{1}{n!}\,[P_S(E,\alpha)]^n\,\exp[-P_S(E,\alpha)]. \tag{21}$$

Using the free-electron-gas dielectric function and carrying out the integration in Eq. (20), we can get

$$P_S(E,\alpha)=\frac{\pi}{4\sqrt{2E}}\,\frac{1}{\cos\alpha}. \tag{22}$$

It shows that $P_S(E,\alpha)$ is proportional to $(\cos\alpha)^{-1}$. Equation (22) indicates that the influence of surface excitations on surface electron spectroscopies might be quite significant for low-energy electrons at large escape angles. This angular dependence has been verified experimentally for large α value ($\sim$85°).[38] Besides, Eq. (22) reveals that $P_S(E,\alpha)$ is proportional to $1/\sqrt{E}$. This energy dependence is the same as the case of electrons transmitted through thin films reported by Ritchie.[2]

If the dielectric function $\varepsilon(\mathbf{q},\omega)$ of the solid is known, Eqs. (15) and (19) can be used to calculate the bulk DIIMFP and DSEP. The model dielectric function developed in previous work is used to investigate the substantial properties of the bulk DIIMFP and DSEP. Here we present a brief synopsis for the purpose of completeness. The sum-rule constrained model dielectric function which combines the optical oscillator strength modeling (zero momentum transfer) and an algorithm for its extension to the $q>0$ region is used, i.e.,[5,25,39]

$$\varepsilon(q,\omega)=\varepsilon_b-\sum_j\frac{A_j}{\omega^2-(\omega_j+q^2/2)^2+i\omega\gamma_j}, \tag{23}$$

where ε_b is the background dielectric constant due to the effect of polarizable ion cores and A_j, γ_j, and ω_j are, respectively, the oscillator strength, damping coefficient, and excitation energy, all associated with the jth oscillator. The approximation adopted in Eq. (23) for the q-dependence works correctly at both extremes of momentum transfer, i.e., at the optical limit, $q\rightarrow 0$, and for the Bethe ridge region, $q\rightarrow\infty$.[39] Although density-function theory[40,41] and experimental measurements show that the surface plasmon dispersion is negative at small Q, the exact dependence of the dielectric function on momentum transfer is seldom known. Equation (12) reveals that the range of integration over Q is rather large for electron energies larger than a few hundred eV. Due to a large range of integration over Q, the universal Bethe surface dominates the scattering cross section. In other words, a slight negative dispersion should not have a strong effect on the final calculations of the DIIMFP and IMFP.[5,6] The parameters in Eq. (23) have been obtained in previous works[5,10,15] by a fit of Eq. (23) to optical data for a number of solids and verified by checking the constraints of sum rules.

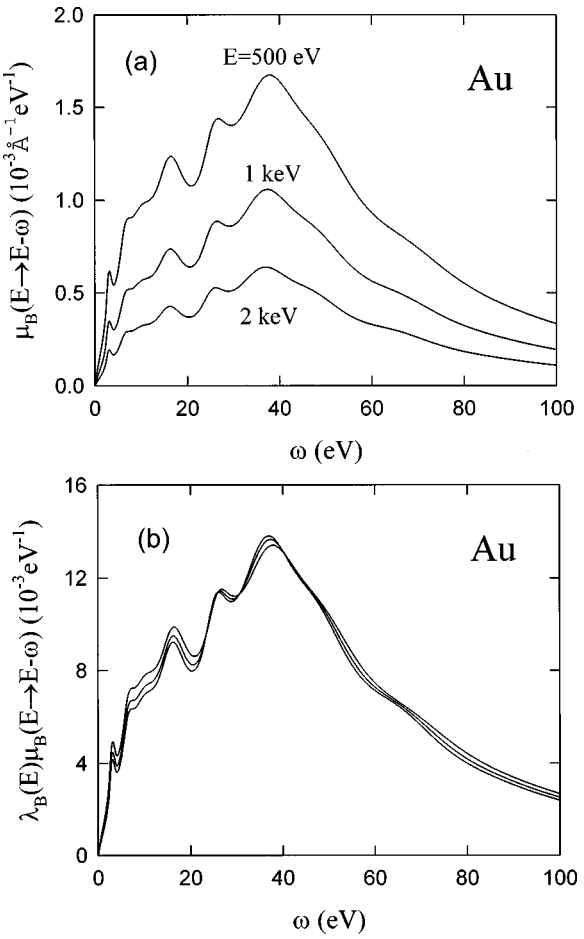

FIG. 1. (a) $\mu_B(E\rightarrow E-\omega)$ in Au for electrons at different energies. (b) $\lambda_B(E)\mu_B(E\rightarrow E-\omega)$ calculated at the same primary electron energies as in (a).

With the model dielectric function, we have calculated the bulk DIIMFP and DSEP. Figure 1(a) shows $\mu_B(E\rightarrow E-\omega)$ evaluated from Eq. (15) for electrons with various energies in Au. Although the bulk DIIMFP in general decreases with increasing the electron energy, the structures and peak positions of the bulk DIIMFP are not sensitive to variation in E. Therefore, one might expect the energy-loss dependence of the product $\lambda_B(E)\mu_B(E\rightarrow E-\omega)$ is nearly the same for dif-

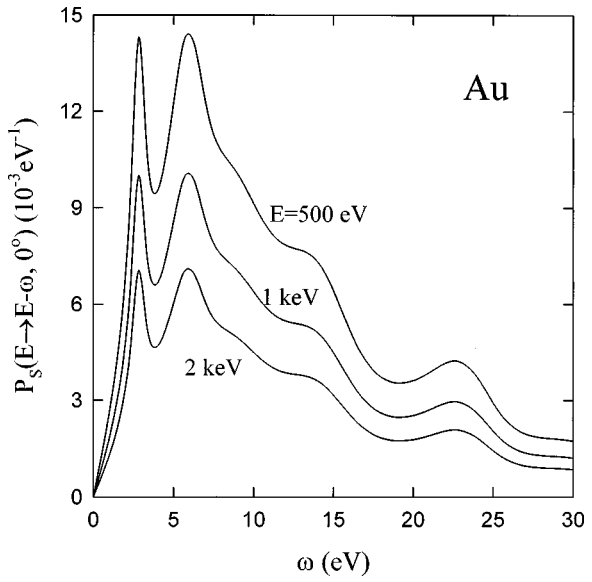

FIG. 2. A plot of the DSEP in Au for electrons at different energies.

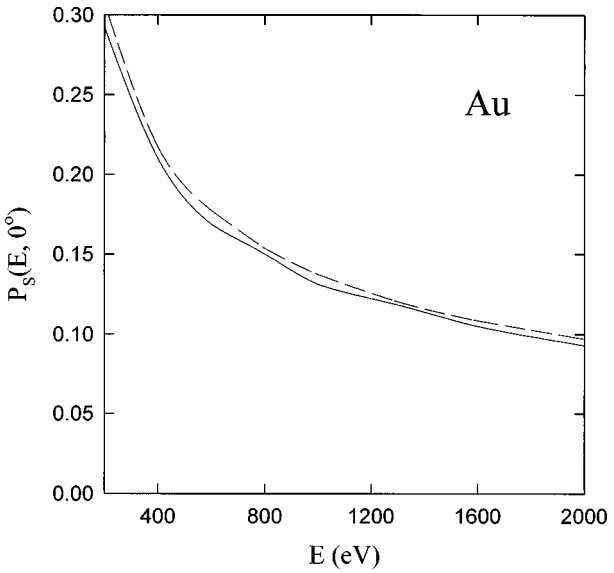

FIG. 3. A plot of the SEP as a function of the electron energies in Au. The solid and dashed curves are, respectively, results calculated with the sum-rule constraint model dielectric function and free-electron-gas model.

ferent electron energies due to the fact that the equality $\int_0^E d\omega \lambda_B(E)\mu_B(E\rightarrow E-\omega)=1$ holds according to Eq. (18).[42] Figure 1(b) shows that this is indeed the case. Based on this property, the product $\lambda_B(E)\mu_B(E\rightarrow E-\omega)$ can be practically expressed as

$$\lambda_B(E)\mu_B(E\rightarrow E-\omega)=\mu_B^0(\omega), \tag{24}$$

where $\mu_B^0(\omega)$ is independent of E and represents a normalized probability density function for bulk excitation. The probability density function $\mu_B^0(\omega)$ is one of the fundamental ingredients in Monte Carlo simulations.[43–45] For convenience, we call $\mu_B^0(\omega)$ the ''reduced DIIMFP'' hereafter.

Figure 2 depicts the energy loss dependence of the DSEP for normal incident electrons with various energies in Au. This DSEP includes the total surface effects for a electron penetrating through the effective region of surface excitations, which is about 3–6 Å for a 1-keV electron. It is seen that surface excitations contribute largely at small energy losses as compared to bulk excitations. Similar to the property of $\mu_B(E\rightarrow E-\omega)$, the structures and peak positions of $P_S(E\rightarrow E-\omega,\alpha)$ are also insensitive to variation in E. The calculated results show that the amplitude of $P_S(E\rightarrow E-\omega,\alpha)$ is approximately proportional to $1/\sqrt{E}$, as it may be appreciated in Fig. 3. This tendency coincides with the prediction of the free-electron-gas model derived in Eq. (22). In other words, the distribution of $\sqrt{E}P_S(E\rightarrow E-\omega,\alpha)$ is almost independent of E. This characteristic enables us to separate E dependence from $P_S(E\rightarrow E-\omega,\alpha)$ and to write

$$P_S(E\rightarrow E-\omega,\alpha)=\frac{1}{\sqrt{E}}P_S^0(\omega,\alpha). \tag{25}$$

Hereafter we call $P_S^0(\omega,\alpha)$ the ''reduced DSEP.''

Detailed knowledge of the bulk DIIMFP and DSEP is important for quantitative analysis by surface electron spectroscopies.[5,25,46] Equations (15) and (19) can be employed to calculate inelastic scattering cross sections when the dielectric-response function of the particular solid is known in detail with respect to the energy transfer. However, literature data for dielectric-response functions are usually not available. Therefore it is of high interest to be able to obtain the DIIMFP and DSEP experimentally. It can be seen later that Eqs. (24) and (25) play a practical role in determining such cross sections from REELS data.

III. DERIVATION OF DIIMFP AND DSEP FROM REELS SPECTRA

Solution of the space-energy-angular-transport problem cannot be obtained analytically because of the complicated angular and energy dependence of the cross sections. However, the energy loss in an elastic scattering is always at least two orders of magnitude smaller than the average loss in an inelastic event. On the other hand, the characteristic length for deflection in an inelastic scattering is usually about two orders of magnitude larger than the corresponding quantity for elastic collision. Therefore, it is reasonable to assume that only elastic interactions contribute to the angular deflection and only inelastic interactions contribute to the energy loss. Within this approximation the energy and angular distribution of reflected electrons $J(E_0,\underline{\Omega}_0;\underline{E},\underline{\Omega})dEd^2\Omega$ with initial incident energy E_0 and direction $\underline{\Omega}_0$ is given by[47,48]

$$J(E_0,\underline{\Omega}_0;E,\underline{\Omega})=\int dRQ(E_0,\underline{\Omega}_0,x=0;R,\underline{\Omega}) \times G(E_0,\underline{\Omega}_0,R;E,\underline{\Omega}), \tag{26}$$

where $G(E_0,\underline{\Omega}_0,R;E,\underline{\Omega})$ is the energy distribution of an electron with initial energy E_0 and direction $\underline{\Omega}_0$ after having traveled the path length R in the solid; $Q(E_0,\underline{\Omega}_0,x;R,\underline{\Omega})$ is the angular and path length distribution of an electron with a initial energy E_0 and direction $\underline{\Omega}_0$ to pass a plane at depth x in a direction $(\underline{\Omega},d^2\Omega)$ after having traveled the path length R in the solid.

Based on the $P1$ approximation to the Boltzmann transport equation, the path length distribution for electrons measured in a REELS experiment is approximately given by[49]

$$Q(E_0,\overline{\mathbf{\Omega}}_0,x=0;R,\overline{\Omega})=A(\overline{\Omega}_0,\overline{\Omega})e^{-R/L}, \tag{27}$$

where $A(\overline{\Omega}_0,\overline{\Omega})$ is the angular distribution and the characteristic attenuation length $L\gg\lambda_B$. Recently, it was pointed by Pázsit and Chakarova[50] that, for certain elements and energies, the path length distribution is not monotonic. However, using Monte Carlo simulation on the basis of quasielastic model we found that Eq. (27) can be roughly used to describe the path length distribution in most cases of REELS experiments. Nevertheless, the more accurate characteristic attenuation length must be obtained by resorting to the Monte Carlo simulation.[24] With Eq. (27) the energy spectrum is then given by

$$J(E_0,\overline{\Omega}_0;E,\overline{\Omega})=A(\overline{\Omega}_0,\overline{\Omega})\int e^{-R/L}G(E_0,\overline{\Omega}_0,R;E,\overline{\Omega})dR. \tag{28}$$

Under the condition of neglecting surface effects, the energy loss distribution is often given by Landau's formula:[51]

$$G_L(E_0,R;E)=\frac{1}{2\pi}\int_{-\infty}^{\infty}ds\ \exp[is\omega-R\Sigma(E_0;s)], \tag{29}$$

with

$$\Sigma(E_0;s)=\int_0^{\infty}d\omega\mu_B(E_0\rightarrow E_0-\omega)[1-\exp(-is\omega)]$$

$$=\frac{1}{\lambda_B(E_0)}-\tilde{\mu}_B(E_0;s), \tag{30}$$

where $\omega=E_0-E$. $\tilde{\mu}_B(E_0;s)$ is the Fourier transform of $\mu_B(E_0\rightarrow E_0-\omega)$ with respect to ω.

The energy-loss distribution contributed by surface excitations can be in terms of the DSEP. Note that the DSEP is the probability for a single loss event. For the total surface loss spectrum, we therefore have to sum over all multiple loss events using[5,52–54]

$$G_S(E_0,\alpha;E)=\int_0^{\infty}ds\ \exp[is\omega-\Xi(E_0,\alpha;s)], \tag{31}$$

and

$$\Xi(E_0,\alpha;s)=\int_0^{\infty}d\omega P_S(E_0\rightarrow E_0-\omega,\alpha)[1-\exp(-is\omega)]$$

$$=P_S(E_0,\alpha)-\tilde{P}_S(E_0,\alpha;s), \tag{32}$$

where $\tilde{P}_S(E_0;\alpha;s)$ is the Fourier transform of $P_S(E_0\rightarrow E_0-\omega,\alpha)$ with respect to ω. Expanding the factor $G_S(E_0,\alpha;E)$ in Eq. (31), we can find

$$G_S(E_0,\alpha;E)$$

$$=e^{-P_S(E_0,\alpha)}\Big[\delta(E_0-E)+P_S(E_0\rightarrow E,\alpha)$$

$$+\frac{1}{2!}\int P_S(E_0\rightarrow E',\alpha)$$

$$\times P_S(E'\rightarrow E,\alpha)dE'+\cdots\Big], \tag{33}$$

where the first, second, third, etc. terms in the bracket represent, respectively, energy-loss flux due to a zero surface plasmon, a surface plasmon, and two surface plasmons, etc. This expression indicates that $G_S(E_0,\alpha;E)$ in Eq. (31) includes overall multiple loss events contributed by surface effects.

With the convolution approach, we can incorporate surface effects into the Landau formula and obtain the total-energy-loss distribution

$$G(E_0,\alpha_I,R;E,\alpha_R)=\int_E^{E_0}\int_{E''}^{E_0}G_S(E_0,\alpha_I;E')$$

$$\times G_L(E',R;E'')G_S(E'',\alpha_R;E)dE'dE'', \tag{34}$$

where α_I and α_R are the angle between the electron velocity and positive z axis for the incident and the reflected electrons. The product term on the right-hand side of Eq. (34) implies that an electron of initial energy E_0 losses the energy E_0-E' due to surface effects of the incident process, losses the energy $E'-E''$ due to bulk effects of the transport in the solid, and loss the energy $E''-E$ due to surface effects of the reflected process.

From the convolution theorem of Fourier transform and Eqs. (29) and (31), $G(E_0,\alpha_I,R;E,\alpha_R)$ can be written as

$$G(E_0,\alpha_I,R;E,\alpha_R)=\frac{1}{2\pi}\int_{-\infty}^{\infty}ds\ \exp[is\omega-R\Sigma(E_0;s)$$

$$-\Xi(E_0,\alpha_I;s)-\Xi(E_0,\alpha_R;s)]. \tag{35}$$

Using Eqs. (30) and (32) and expanding $G(E_0,\alpha_I,R;E,\alpha_R)$ in Eq. (35), we can find

$$G(E_0,\alpha_I,R;E,\alpha_R)$$

$$=\exp\{-[R/\lambda_B(E_0)+P_S(E_0,\alpha_I)+P_S(E_0,\alpha_R)]\}$$

$$\times\Big\{\delta(E_0-E)+R\mu_B(E_0\rightarrow E)+[P_S(E_0\rightarrow E,\alpha_I)$$

$$+P_S(E_0\rightarrow E,\alpha_R)]+\int R\mu_B(E_0\rightarrow E')$$

$$\times[P_S(E_0\rightarrow E',\alpha_I)+P_S(E_0\rightarrow E',\alpha_R)]dE'$$

$$+\frac{R^2}{2!}\int\mu_B(E_0\rightarrow E')\mu_B(E'\rightarrow E)dE'+\cdots\Big\}, \tag{36}$$

where the first, second, third, etc. terms in the curly bracket represent, respectively, energy-loss flux due to zero plasmon, a bulk-plasmon, a surface plasmon, a bulk plasmon and a

surface plasmon, and two bulk plasmons, etc. This expression indicates that $G(E_0,\alpha_I,R;E,\alpha_R)$ in Eq. (36) includes over all multiple loss events contributed by bulk and surface excitations.

Substituting Eq. (35) into Eq. (28) and carrying out the integration over R, we obtain

$$J(E_0,\overline{\Omega}_0;E,\overline{\Omega})=\frac{L\lambda_B(E_0)}{L+\lambda_B(E_0)}\,I(\overline{\mathbf{\Omega}}_0,\overline{\Omega})e^{-P_S(E_0,\alpha_I,\alpha_R)}\times\int_{-\infty}^{\infty}\frac{ds}{2\pi}\exp[i(E_0-E)s]\times\left\{\frac{\exp[\tilde{P}_S(E_0,\alpha_I,\alpha_R;s)]}{1-\dfrac{L\lambda_B(E_0)}{L+\lambda_B(E_0)}\,\tilde{\mu}_B(E_0;s)}\right\},\tag{37}$$

where

$$P_S(E_0,\alpha_1,\alpha_R)=P_S(E_0,\alpha_I)+P_S(E_0,\alpha_R),\tag{38}$$

and

$$\tilde{P}_S(E_0,\alpha_I,\alpha_R;s)=\tilde{P}_S(E_0,\alpha_I;s)+\tilde{P}_S(E_0,\alpha_R;s).\tag{39}$$

Usually, only relative intensity measurements will be performed. Hence, introducing the relative electron flux density distribution

$$j(E_0,\overline{\Omega}_0;E,\overline{\Omega})=\left[\frac{L\lambda_B(E_0)}{L+\lambda_B(E_0)}\,I(\overline{\Omega}_0,\overline{\Omega})e^{-P_S(E_0,\alpha_I,\alpha_R)}\right]^{-1}\times J(E_0,\overline{\Omega}_0;E,\overline{\Omega}),\tag{40}$$

we can write Eq. (39) in the general form

$$j(E_0,\alpha_I;E,\alpha_R)=\int_{-\infty}^{\infty}\frac{ds}{2\pi}\exp[i(E_0-E)s]\times\left\{\frac{\exp[\tilde{P}_S(E_0,\alpha_I,\alpha_R;s)]}{1-\dfrac{L\lambda_B(E_0)}{L+\lambda_B(E_0)}\,\tilde{\mu}_B(E_0;s)}\right\}.\tag{41}$$

It is noted that the dependence of the electron-energy distribution on the incident and reflected angles is consequent on surface effects.

The algorithm developed by Tougaard and Chorkendorff[21] in determining experimental differential inelastic-electron-scattering cross sections $K(E_0\rightarrow E_0-\omega)$ from REELS spectra is based on the following formula:

$$j(E_0;E)=\int_{-\infty}^{\infty}\frac{ds}{2\pi}\,\frac{\exp[i(E_0-E)s]}{1-\dfrac{L\lambda(E_0)}{L+\lambda(E_0)}\,\tilde{K}(E_0;s)},\tag{42}$$

where $\tilde{K}(E_0;s)$ is the Fourier transform of $K(E_0\rightarrow E_0-\omega)$ with respect to ω, and $\lambda(E_0)$ is defined as

$$\lambda(E_0)=\int_0^{E_0}K(E_0\rightarrow E_0-\omega)d\omega.\tag{43}$$

From Eqs. (41) and (42) the relationship between the experimental $K(E_0\rightarrow E_0-\omega)$ and the bulk DIIMFP and DSEP is given by

$$1-\frac{L\lambda(E_0)}{L+\lambda(E_0)}\,K(E_0;s)=\left[1-\frac{L\lambda_B(E_0)}{L+\lambda_B(E_0)}\,\tilde{\mu}_B(E_0;s)\right]\times\exp[-\tilde{P}_S(E_0,\alpha_1,\alpha_R;s)].\tag{44}$$

The angular dependence of $P_S(E_0\rightarrow E_0-\omega,\alpha)$ results in the fact that the experimentally obtained $K(E_0\rightarrow E_0-\omega)$ depends on both the angle of incidence and exist angle of the electrons. Taking $P_S(E_0\rightarrow E_0-\omega,\alpha)=0$, i.e., neglecting the surface effects, we can get $\lambda=\lambda_B$ and $K(E_0\rightarrow E_0-\omega)=\mu_B(E_0\rightarrow E_0-\omega)$. This is reason why $K(E_0\rightarrow E_0-\omega)$ determined from REELS spectra is often treated as a single scattering cross section.

In general $L\gg\lambda$,[21–23] therefore Eq. (44) can be simplified as

$$1-\lambda(E_0)K(E_0;s)=[1-\lambda_B(E_0)\tilde{\mu}_B(E_0;s)]\times\exp[-\tilde{P}_S(E_0,\alpha_1,\alpha_R;s)].\tag{45}$$

Equation (45) indicates that the cross section $\lambda(E_0)K(E_0\rightarrow E_0-\omega)$ obtained from REELS data cannot expressed as a linear combination of pure bulk and pure surface components. Introducing Eqs. (24) and (25) into Eq. (45), we can obtain

$$1-\lambda(E_0)K(E_0;s)=[1-\mu_B^0(s)]\times\exp[-\tilde{P}_S^0(\alpha_1,\alpha_R;s)/\sqrt{E_0}],\tag{46}$$

with

$$\tilde{P}_S^0(\alpha_1,\alpha_R;s)=\tilde{P}_S^0(\alpha_1;s)+\tilde{P}_S^0(\alpha_R;s)\tag{47}$$

where $\mu_B^0(s)$ and $\tilde{P}_S^0(\alpha;s)$ are, respectively, the Fourier transform of $\mu_B^0(\omega)$ and $P_S^0(\omega,\alpha)$ with respect to ω.

To directly determine the bulk DIIMFP and DSEP from REELS data, we use the experimental $\lambda(E_0)K(E_0;s)$ obtained at two different primary electron energies, $E_0=E_1$ and $E_0=E_2$. From Eq. (46) we can write the pair equation

$$1-\lambda(E_1)K(E_1;s)=[1-\mu_B^0(s)]\times\exp[-\tilde{P}_S^0(\alpha_1,\alpha_R;s)/\sqrt{E_1}]\tag{48}$$

and

$$1-\lambda(E_2)K(E_2;s)=[1-\mu_B^0(s)]\times\exp[-\tilde{P}_S^0(\alpha_1,\alpha_R;s)/\sqrt{E_2}].\tag{49}$$

Taking the logarithm of both sides of Eqs. (48) and (49), after some algebra, we can obtain

$$\tilde{P}_S^0(\alpha_1,\alpha_R;s)=\frac{\sqrt{E_1E_2}}{\sqrt{E_2}-\sqrt{E_1}}\ln\left[\frac{1-\lambda(E_2)K(E_2;s)}{1-\lambda(E_1)K(E_1;s)}\right], \tag{50}$$

and

$$\mu_B^0(s)=1-\exp\left\{\frac{\sqrt{E_2}\ln[1-\lambda(E_1)K(E_1;s)]-\sqrt{E_1}\ln[1-\lambda(E_2)K(E_2;s)]}{\sqrt{E_2}-\sqrt{E_1}}\right\}. \tag{51}$$

Therefore, Eqs. (50) and (51) can be used to determine the bulk DIIMFP and DSEP by means of the fast Fourier transform (FFT) algorithm, provide that $\lambda(E_1)K(E_1;s)$ and $\lambda(E_2)K(E_2;s)$ are given.

To avoid significant errors introduced by the approximations in Eqs. (24) and (25), the appropriate ranges for E_1 and E_2 are around 0.4–1.5 and 2–10 keV, respectively. If both E_1 and E_2 are higher than 3 keV, the surface effects may be too small to be used in Eqs. (50) and (51). On the other hand, the first Born approximation presented here needs to be modified as the electron energy lower than 0.3 keV.

IV. RESULTS AND DISCUSSION

For illustrating the utility of the present model, the experimental $\lambda(E_0)K(E_0\rightarrow E_0-\omega)$ obtained by Tougaard and Kraaer[23] was used to derive the bulk DIIMFP and DSEP. We chose $E_1=1$ and $E_2=2$ keV because of the existence of experimental data and the fact that most electron spectrometers in surface analysis equipment only operate up to ~2 keV. Figures 4(a) and 4(b) show the experimental $\lambda(E_0)K(E_0\rightarrow E_0-\omega)$ at 1 and 2 keV, respectively. Employing the Fourier transform of these experimental data into Eqs. (50) and (51) and then taking the inverse Fourier transform of $\mu_B^0(s)$ and $\tilde{P}_S^0(\alpha_1,\alpha_R;s)$, the bulk DIIMFP and DSEP can be derived. Note that the only input in the present determination of the bulk DIIMFP and DSEP is the experimentally obtained $\lambda(E_0)K(E_0\rightarrow E_0-\omega)$ at two different primary electron energies. Thus, no adjustable parameters have been applied. The derived $\mu_B^0(\omega)$ is shown in Fig. 4(c). For comparison, the theoretical results computed with the model dielectric function of Eq. (23), using dielectric function parameters found by Tougaard and Kraaer in Ref. 23, is also shown in the same figure. Here we just plotted the theoretical result for electrons of 1 keV because the reduced DIIMFP is almost independent of the electron kinetic energy, as shown in Fig. 1(b). The good agreement obtained between the values derived from experimental data and the theoretical calculations confirms our quantitative analysis for REELS spectra and validates our theoretical model for inelastic interactions near surfaces. On the other hand, the derived DSEP is shown in Fig. 5. The theoretical results calculated with Eqs. (19) and (23) are also shown for comparison. It can be seen that both the morphology and numerical values of the curves compare favorably. With the same algorithm, the reduced DIIMFP for Cu was also derived and shown in Fig. 6. Here again, the results derived from the REELS data agree closely with the theoretical results.

The bulk DIIMFP is directly related to the complex dielectric function of the specimen, as given in Eq. (15). Since derivation of the bulk DIIMFP from experimental REELS data has been achieved, it is suggested that the obtained results be applied to determine the dielectric function and thus to determine the optical properties of solids. Although a typical energy-loss spectrum cannot have energy resolution as good as that achievable using light-optical spectroscopy, its energy range can be much greater; energy losses equivalent to the visible, ultraviolet, and soft x-ray region may be recorded in the same experiment. Therefore, we hope that the present theoretical model can be used to extract the more quantitative information from REELS experiments in the future.

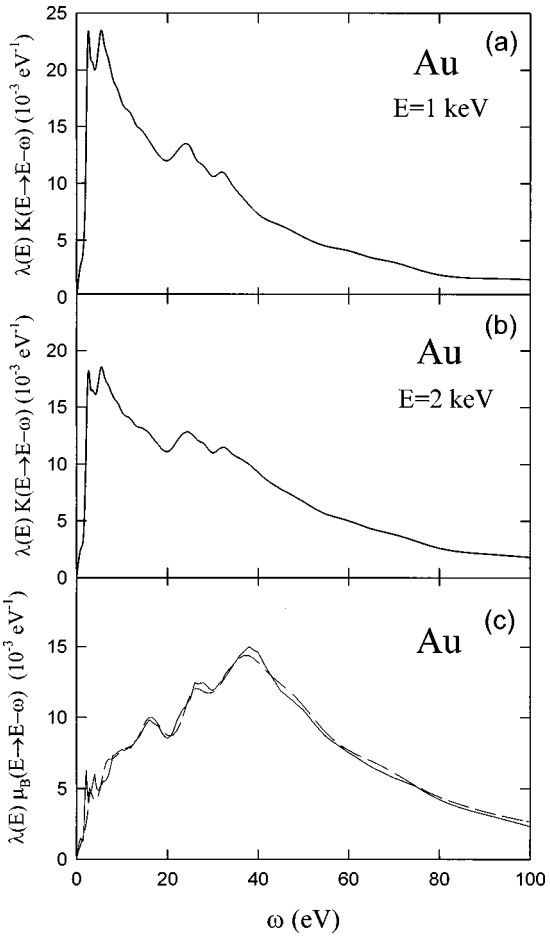

FIG. 4. (a) and (b) the experimental $\lambda(E_0)K(E_0\rightarrow E_0-\omega)$ in Au at 1 and 2 keV (Ref. 23). (c) Solid line: the bulk DIIMFP determined from (a) and (b) with Eq. (51); dashed line: the theoretical results computed with the model dielectric function of Eq. (23).

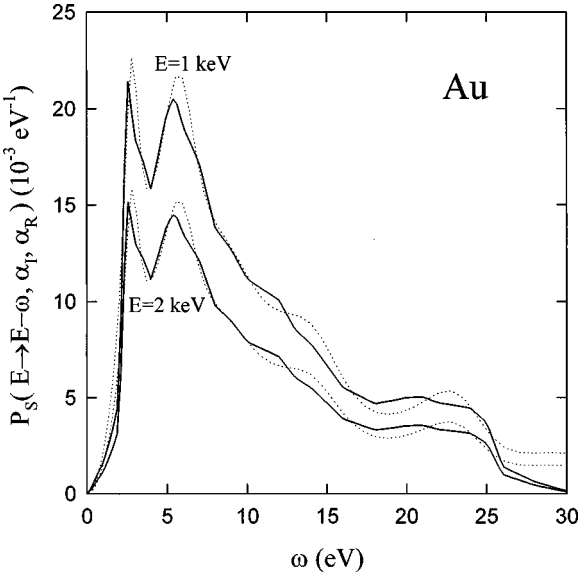

FIG. 5. Solid line, the DSEP determined from Figs. 4(a) and 4(b) with Eq. (50); dashed line, the theoretical results computed with the model dielectric function of Eq. (23), using dielectric function parameters found by Tougaard and Kraaer in Ref. 23.

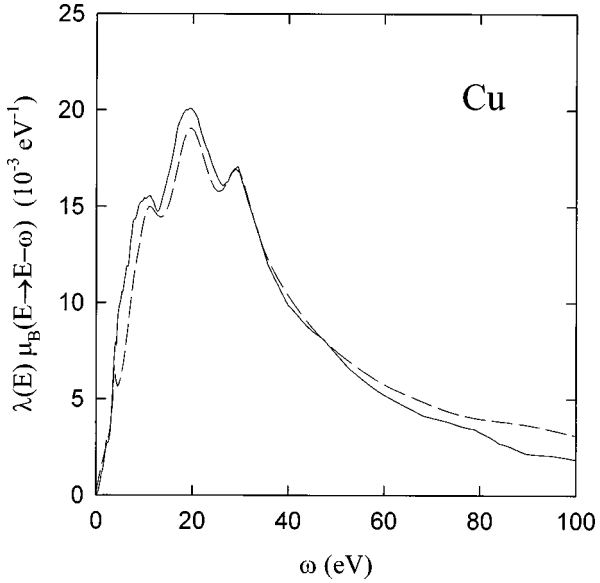

FIG. 6. Solid line, the bulk DIIMFP in Cu determined from experimental $\lambda(E_0)K(E_0 \rightarrow E_0-\omega)$ at 1 and 2 keV (Ref. 23) with Eq. (51); dashed line, the theoretical results computed with the model dielectric function of Eq. (23).

V. CONCLUSIONS

The inelastic scattering cross section of electrons with solid surfaces has been derived with the approach of dielectric response theory. It is shown that the inelastic scattering cross section includes the bulk DIIMFP and DSEP. The relation between the experimental $K(E_0 \rightarrow E_0-\omega)$ from REELS data and the bulk DIIMFP and DSEP has been obtained through including surface effects into the Landau formula. Based on this relation, a method to derive the bulk DIIMFP and DSEP from REELS data has been proposed. The only input is the experimental $K(E_0 \rightarrow E_0-\omega)$ at two different primary electron energies. With the proposed method and FFT algorithm, the bulk DIIMFP and DSEP have been determined from experimental $K(E_0 \rightarrow E_0-\omega)$ for Au and Cu. Without any adjustable parameters, excellent agreement was found between the determined results and theoretical results calculated with the sum-rule constraint model dielectric function.[5,10,25]

*Fax: (886-35) 773947. Electronic address: yfchen@pidc.gov.tw

[1] J. Lindhard, K. Dan. Vidensk. Selsk. Mat. Fys. Medd. **28**, 8 (1954).
[2] R. H. Ritchie, Phys. Rev. **106**, 874 (1957).
[3] F. Flores and F. Garcia-Moliner, J. Phys. C **12**, 907 (1979).
[4] F. Yubero and S. Tougaard, Phys. Rev. B **46**, 2486 (1992).
[5] Y. F. Chen and Y. T. Chen, Phys. Rev. B **53**, 4980 (1996).
[6] Z. J. Ding, Phys. Rev. B **55**, 9999 (1997).
[7] R. H. Ritchie and A. Howie, Philos. Mag. **36**, 463 (1977).
[8] D. R. Penn, Phys. Rev. B **35**, 482 (1987).
[9] Z. J. Ding and R. Shimizu, Surf. Sci. **222**, 313 (1989).
[10] Y. F. Chen and C. M. Kwei, Surf. Sci. **364**, 131 (1996).
[11] J. Daniels, Z. Phys. **227**, 234 (1969).
[12] C. Wehenkel and B. Gauthe, Phys. Status Solidi B **64**, 515 (1974).
[13] L. A. Feldkamp, L. C. Davis, and M. B. Stearns, Phys. Rev. B **15**, 5535 (1977).
[14] R. F. Egerton, *Electron Energy-Loss Spectroscopy in the Electron Microscope* (Plenum, New York, 1986).
[15] C. J. Powell and J. B. Swan, Phys. Rev. **115**, 869 (1959).
[16] J. L. Robin and J. B. Swan, Proc. Phys. Soc. Jpn. **76**, 857 (1960).
[17] J. Thirwell, Proc. Phys. Soc. Jpn. **91**, 552 (1967).
[18] Y. Ohno, Phys. Rev. B **39**, 8209 (1989).
[19] G. Chiarello, E. Colavita, M. De Crescenzj, and S. Nannarone, Phys. Rev. B **29**, 4878 (1984).
[20] J. C. Ingram, K. W. Webesny, and J. E. Pemberton, Appl. Surf. Sci. **44**, 279 (1990).
[21] S. Tougaard and I. Chorkendorff, Phys. Rev. B **35**, 6570 (1987).
[22] S. Tougaard, Surf. Interface Anal. **11**, 453 (1988).
[23] S. Tougaard and J. Kraaer, Phys. Rev. B **43**, 1651 (1991).
[24] Y. F. Chen, J. Vac. Sci. Technol. A **13**, 2665 (1995).
[25] Y. F. Chen, Surf. Sci. **345**, 213 (1996).
[26] H. Yoskikawa, Y. Irokawa, and R. Shimizu, J. Vac. Sci. Technol. A **13**, 1984 (1995).
[27] T. Nagotomi, Z. J. Ding, and R. Shimizu, Surf. Sci. **359**, 163 (1996).
[28] J. A. D. Matthew and P. R. Underhill, J. Electron Spectrosc. Relat. Phenom. **14**, 371 (1978).
[29] V. M. Dwyer and J. A. D. Matthew, Surf. Sci. **193**, 549 (1988).
[30] F. Yubero, J. M. Sanz, B. Ramskov, and S. Tougaard, Phys. Rev. B **53**, 9719 (1996).
[31] R. H. Ritchie and A. L. Marusak, Surf. Sci. **4**, 234 (1966).
[32] J. Heinrichs, Phys. Rev. B **8**, 1346 (1973).
[33] D. Chan and P. Richmond, J. Phys. C **9**, 163 (1976).
[34] H. G. Eriksson, B. R. Karlsson, and K. A. I. L. Wijewardena, Phys. Rev. B **31**, 843 (1985).
[35] F. J. Garcia de Abajo and P. M. Echenique, Phys. Rev. B **48**, 13 399 (1993).
[36] F. Garcia-Moliner and F. Flores, *Introduction to the Theory of Solid Surfaces* (Cambridge University Press, Cambridge, England, 1979).

[37] Z. Penzar and M. Sunjic, Phys. Scr. **30**, 453 (1984).
[38] H. Raether, in *Excitations of Plasmons and Interband Transitions by Electrons*, edited by G. H. Öhler, Springer Tracts in Modern Physics Vol. 88 (Springer, New York, 1980).
[39] R. H. Ritchie, R. N. Hamm, J. E. Turner, H. A. Wright, and W. E. Bolch, in *Physical and Chemical Mechanisms in Molecular Radiation Biology*, edited by W. A. Glass and M. N. Varma (Plenum Press, New York, 1991), p. 99.
[40] P. J. Feibelman, Prog. Surf. Sci. **12**, 287 (1982).
[41] A. Liebsch, Phys. Rev. B **36**, 7378 (1987).
[42] S. Tougaard, Solid State Commun. **61**, 547 (1987).
[43] J. C. Ashley, J. Appl. Phys. **69**, 674 (1991).
[44] L. Reimer and B. Lödding, Scanning **6**, 128 (1984).
[45] J. M. Fernández-Varea, D. Liljequist, S. Csillag, R. Räty, and F. Salvat, Nucl. Instrum. Methods Phys. Res. B **73**, 447 (1993).
[46] Y. F. Chen, Phys. Rev. B **55**, 5478 (1997).
[47] S. Tougaard and P. Sigmund, Phys. Rev. B **25**, 4452 (1982).
[48] A. L. Tofterup, Phys. Rev. B **32**, 2808 (1985).
[49] A. L. Tofterup, Surf. Sci. **167**, 70 (1986).
[50] I. Pázsit and R. Chakarova, Phys. Rev. B **50**, 13 953 (1994).
[51] L. Landau, J. Phys. (Moscow) **8**, 201 (1944).
[52] A. A. Lucas and M. Sunjic, Phys. Rev. Lett. **26**, 229 (1971).
[53] E. Evans and D. L. Mills, Phys. Rev. B **5**, 4126 (1972).
[54] J. Schilling, Z. Phys. B **25**, 61 (1976).